Investigation of the effects of microplastics on human endometrial cells and cell-to-cell transfer

Nara Kim

Department of Medical Device
Engineering and Management
The Graduate School, Yonsei University

Investigation of the effects of microplastics on human endometrial cells and cell-to-cell transfer

The Master's Thesis
Submitted to the Department of Medical Device Engineering and Management,
the Graduate School of Yonsei University
in partial fulfillment of the requirements for the degree of
Master of Medical Device Engineering and Management

Nara Kim

December 2024

This certifies that the Master's thesis of
Nara Kim is approved.

Thesis Supervisor: SiHyun Cho

Thesis Committee Member #1: Lark Kyun Kim

Thesis Committee Member #2: Wooseok Im

The Graduate School
Yonsei University

December 2024

Acknowledgements

우선 대학교를 졸업하고 아무것도 모르는 상태인 저를 받아 주시고, 지금까지 많은 경험을 할 수 있게 열정적으로 지도해주신 조시현 지도교수님께 깊은 감사의 말씀을 전합니다.

훌륭한 교수님들 밑에서 열심히 지도해주신대로 따라가다 보니 좋은 성과들을 많이 낼 수 있었다고 생각합니다. 이곳에서 습득한 지식 및 실험들을 통해 미래의 바이오산업 발전에 기여할 수 있는 사람이 되도록 노력하겠습니다.

바쁘신 와중에 자문위원으로 많은 조언을 주신 김락균 교수님과 석사 생활 동안 전반적으로 과제를 이끌어 주시고, 연구 시야를 넓혀, 보다 더 많은 경험 및 발전할 수 있게 도와주신 임우석 연구교수님께도 깊은 감사의 말씀 전합니다.

약 2년 6개월 간의 연구원 및 대학원생 시절 동안 도움을 주신 산부인과 연구실 구성원분들께도 모두 감사드립니다. 실험실 생활에 신경 써 주시고, 사기가 떨어지려 할 때마다 맛있는 밥을 사주어 사기를 북돋아 주신 이민정 박사님께도 깊은 감사의 말씀을 전합니다.

마지막으로, 학위기간동안 항상 옆에서 응원해주고 고민상담해 준 가족들과 친구들에게 진심으로 감사의 말씀을 전합니다. 모두의 도움과 응원 덕분에 큰 걱정과 문제없이 생활할 수 있었습니다.

돌이켜보면, 처음에 막연하고 막막하고 걱정이 많았던 석사학위과정이 막상 부딪혀보니 오히려 많은 경험이 되어 유익하고 값진 경험이었던 것 같습니다. 이 경험을 토대삼아 주변 분들의 가르침 및 도움에 항상 감사할 줄 알고, 막막해 보이는 일도 되레 겁먹고 피하지 않는, 끊임없이 도전하고 발전하는 사람이 되겠습니다.

2024년 12월
김나라 올림

CONTENTS

LIST OF FIGURES

ABSTRACT

Investigation of the effects of microplastics on human endometrial cells and cell-to-cell transfer

Nara Kim

Department of Medical Device Engineering and Management
The Graduate School, Yonsei University

(Directed by Professor SiHyun Cho)

Nanoplastics (NPs) and microplastics (MPs) have recently emerged as a global concern. However, the effects of polystyrene (PS)-NPs and MPs on the female endometrium remain unclear. The aim of this study was to develop a suitable in vitro exposure protocol for PS-NPs and MPs, using different plastic dimensions and concentrations, and to investigate the potential toxic effects of PS-NPs and MPs on human endometrial stromal cells (ESCs), as well as the intercellular transfer of MPs. In particular, smaller plastic particles, such as 100 nm PS-NPs and 1 μm PS-MPs, showed a greater tendency for cellular uptake compared to larger 5 μm PS-MPs. These tiny plastic particles were found to induce significant changes in cell

morphology and cell death at concentrations greater than 100 μg/mL over a 24-hour period. In addition, using confocal microscopy and real-time imaging, we observed that MPs not only accumulate in the nucleus and cytoplasm of ESCs, but also migrate between cells via extracellular vesicles (EVs). EVs are small membrane-bound particles surrounded by a lipid bilayer that are released by various cell types and play a critical role in inter- and intracellular communication by facilitating the exchange of proteins, nucleic acids, and lipids between cells. The study revealed a significantly higher rate of internalization, with a clear relationship between plastic particle size and the extent of penetration into the nucleus and cytoplasm. In addition, our research showed that exposure to 100 nm PS-NPs resulted in decreased cell proliferation and induced apoptosis. This study is groundbreaking in demonstrating that both 100 nm PS-NPs and 1 μm PS-MPs dynamically accumulate within ESCs, leading to either cell death or reduced proliferation at specific concentrations. These results suggest potential adverse effects on fertility and reproductive health and highlight the need for further research to elucidate the precise underlying molecular mechanisms.

Key words: Microplastic, Nanoplastic, Polystyrene, Internalization, Endometrial stromal cells, Cytotoxicity, Extracellular vesicles, transfer

Investigation of the effects of microplastics on human endometrial cells and cell-to-cell transfer

Nara Kim

Department of Medical Device Engineering and Management
The Graduate School, Yonsei University

(Directed by Professor SiHyun Cho)

I. INTRODUCTION

Plastics have become an increasingly important part of human life, with global production expected to reach approximately 367 million tons in 2020 and increase by 29% by 2028 [1,2]. This increase in use and disposal, and the fact that plastics do not break down easily, have resulted in significant releases of plastics into aquatic and terrestrial ecosystems, which have accumulated over the long term in the global oceans [3-5]. Plastic waste takes more than a century to degrade and break down into microplastics (MP) and nanoplastics (NP), particles smaller than 5 mm and 1 μm in diameter, respectively, causing serious environmental concerns [6-8].

The most common forms of MPs include polyethylene terephthalate (PET), polypropylene (PP), polyethylene (PE), polystyrene (PS), and polyvinyl chloride (PVC) [9]. PS, a plastic

widely used in manufacturing, can generate polystyrene microplastics (PS-MPs) and nanoplastics (PS-NPs) [10]. These particles are now ubiquitous in water, sea salt, seafood, industrial abrasives, and food crops, and enter organisms through consumption [11-13]. Urgent research is needed to understand their full impact on health and the environment. While research has primarily focused on the accumulation of MPs in specific animal tissues and their potential to cause disease, there are limited studies on the cellular changes resulting from MP accumulation, particularly regarding their presence in the cytoplasm and nucleus, and the mechanisms of MP-induced cytotoxicity [14-16].

Extracellular vesicles (EVs) are small membrane-bound particles released by various cell types [17-19]. They play a crucial role in cellular communication by exchanging proteins, nucleic acids and lipids between cells [20-21]. Recent evidence suggests that serum-derived EVs can transport polyethylene terephthalate (PET)-MP and alter EV miRNA content [22]. Furthermore, exposure to plastics increases cellular EV release [23]. Despite numerous reports on the detrimental effects of MP accumulation in cells, the mechanisms of their accumulation and intercellular movement remain unclear.

Infertility remains a significant global reproductive problem [24], with female factors accounting for approximately half of all cases [25]. The human endometrium is critical for embryo implantation and fertility [26]. Although recent studies have identified various MPs in the human endometrium [27], more extensive clinical research is urgently needed to

understand the effects and mechanisms of NPs and MPs on endometrial health.

In this study, we investigated the deposition and accumulation of fluorescence-stained PS-NPs ((FL)PS-NPs) or MPs ((FL)PS-MPs) in ESCs. We also investigated the kinetics of PS-NP or MP deposition and accumulation in live cells using the IncuCyte live- cell imaging system (Sartorius, Göttingen, Germany). In addition, we sought to determine how accumulated PS-MPs move out of cells and into other cells. We examined the presence of PS-MPs in EVs by isolating EVs from cells with (FL)PS-MP accumulation and analyzing them by flow cytometry. We also detected PS-MPs in cells treated with extracted EVs using confocal microscopy and observed PS-MPs entering cells from stained EVs using IncuCyte live-cell imaging. This research provides a foundation for understanding the impact of PS-NPs or MPs on endometrial disease and infertility, as well as the potential cellular effects of MPs.

II. MATERIALS AND METHODS

1. Endometrium Stromal cell culture and Ishikawa cell culture

ESCs were obtained from healthy human eutopic endometrial samples. The tissue was finely minced and digested in phosphate-buffered saline (PBS; Welgene, Gyeongsan, Korea) with 2.0 mg/mL collagenase type I (Gibco, Waltham, MA, USA) for 2 h at 37°C in a 5% CO_2 incubator. After digestion, the cells were filtered through a 40-μm filter (BD Biosciences, San Jose, CA, USA) and collected. After discarding the supernatant, cells were suspended in Dulbecco's modified Eagle's medium/F12 (DMEM/F12; Cytiva, Marlborough, MA, USA) supplemented with 10% fetal bovine serum (FBS; Gibco, Waltham, MA, USA) and 2% penicillin-streptomycin (P/S; Cytiva, Marlborough, MA, USA) in a humid 37°C, 5% CO_2 environment. For subculturing, cells at 80-90% confluence were treated with 2 mL of 0.25% trypsin-EDTA (Gibco, Waltham, MA, USA) for 5 min, and the process was stopped by adding 1 mL of culture medium. Cells from passages 3 to 6 were used for subsequent experiments.

Ishikawa cells were grown in minimum essential medium (MEM)/Earle's balanced salt solution (EBSS; Cytiva, Marlborough, MA, USA) supplemented with 10% fetal bovine serum (FBS) and 2% penicillin-streptomycin (P/S; Cytiva, Marlborough, MA, USA). Cells were maintained in a humid 5% CO_2 atmosphere at 37°C.

2. Cell treatment with plastics

ESCs were plated at 3×10^5 cells per well in 6-well plates and grown to approximately

60% confluence. The medium was then changed to DMEM/F12 containing 100 nm PS-NPs, 1 μm or 5 μm PS-MPs (Merck, Darmstadt, Germany). The cells were then exposed to these particles for 24 h at 37°C in a 5% CO_2 incubator.

3. Cell Proliferation assay

ESCs were seeded at 6×10^3 cells per well in 96-well plates. After 24 h of incubation, the culture medium was replaced with DMEM/F12 containing 100 nm PS-NPs or 1 μm and 5 μm PS-MPs at concentrations ranging from 0 to 10,000 μg/mL. To evaluate cell proliferation, 20 μL Cell Counting Kit-8 (CCK-8; Dojindo, Kumamoto, Japan) was added to each well, followed by incubation at 37°C for 2 h. The absorbance of the supernatant was measured at 450 nm optical density (OD) using a VersaMax microplate reader (Molecular Devices, San Jose, CA, USA).

4. PS particles characterization

Green fluorescent unmodified nanoplastic beads (100 nm, (FL)PS-NPs) and microplastic beads (1 μm, (FL)PS-MPs) were purchased from CD Bioparticles - Drug Delivery Research (NY, USA) for live- cell imaging and confocal fluorescence microscopy. The dimensions, colors, and shapes of these polystyrene (PS) particles were examined using a scanning confocal microscope (LSM 980, Carl Zeiss, Oberkochen, Germany).

5. Live-Cell Imaging analysis

The IncuCyte Live-Cell Analysis System (Sartorius, Göttingen, Germany) was used to capture real-time images of cells at specific intervals over time. Endometrial stromal cells

(ESCs) were plated on poly-L-lysine-coated coverslips (Merck, Darmstadt, Germany). When cells reached approximately 60% confluence, they were treated with 100 μg/mL of 100 nm (FL)PS-NPs or 1 μm (FL)PS-MPs. After treatment, cells were stained with NucSpot Live 650 nuclear stain (Biotium, San Francisco, USA) at a final concentration of 1 μM for 10 min at 37°C in a 5% CO_2 incubator. The samples were then placed in the IncuCyte Live-Cell Analysis System for continuous live-cell imaging.

6. Fixed cell imaging via confocal fluorescence microscopy

Following live-cell imaging, culture medium was gently removed, and cells were fixed using 4% paraformaldehyde (Forbio, Seoul, Korea) on a shaker (Daihan Scientific, Wonju, Korea) at 40 rpm for 15 minutes at ambient temperature. Subsequently, cells were mounted using mounting medium (Dako, Seongnam, Korea) and examined using a confocal microscope (LSM 980, Carl Zeiss, Oberkochen, Germany) equipped with an oil immersion objective (Plan-Apochromat 40x/1.4 oil DIC M27; Carl Zeiss Microscopy, GmbH).

7. Measurement of PS accumulation

To measure intracellular plastic accumulation, fixed ESCs exposed to nano- and microplastics were nuclear stained with NucSpot Live 650 Nuclear Stain prior to mounting. The number of cells containing 1 μm PS-MPs (green) co-stained with NucSpot 650 (red) was tallied and averaged from four randomly selected microscopic fields at 100x magnification using a confocal microscope. For the smaller 100 nm PS-NPs, the number of green PS-NPs co-stained with red NucSpot 650 was averaged from eight randomly

selected fields at 630x magnification, also using a confocal microscope.

8. EVs isolation after PS-MPs treatment of cells

Cells were plated at 3×10^5 cells per well in T25 flasks (SPL, Pochen, Korea) and grown to approximately 60% confluence. The medium was then replaced with MEM/EBSS containing 1% FBS and either 1 μm PS-MPs or 1 μm fluorescent PS-MPs ((FL)PS-MPs) at 1 mg/mL for 24 h at 37°C in a 5% CO_2 incubator. After 24 h, cells were washed three times with PBS, trypsinized, and reseeded into fresh T25 flasks for another 24 h under identical conditions to facilitate isolation of EVs. EVs were extracted using ExoQuick-TC (SBI, Palo Alto, CA, USA) according to the manufacturer's instructions. Briefly, culture medium was centrifuged at 1200 × g for 20 minutes, and 5 mL of the resulting supernatant was mixed with 1 mL of ExoQuick-TC reagent. This mixture was incubated at 4°C for 24 h and then centrifuged at 1500 × g for 30 min. After removal of the supernatant, a final centrifugation at 1500 × g for 5 min yielded precipitated EVs pellets, which were used for subsequent cell treatment and flow cytometry analysis. The remaining cells were fixed with 4% paraformaldehyde for flow cytometry analysis.

9. Flow cytometry assay

Flow cytometric analysis was conducted using a FACS Canto II system (BD Biosciences, San Jose, CA, USA) with FCSalyzer software (version 1.8.0) to detect intracellular PS-MPs or PS-MPs within extracellular vesicles (EVs). Extracted EVs and fixed cells were analyzed for forward scattering (FSC) and side scattering (SSC) using a 488 nm blue laser,

while green fluorescent PS-MPs ((FL)PS-MPs) were excited with a 508 nm blue-green laser. Green fluorescence emissions were collected using a 530/30 nm filter. Flow cytometer settings were optimized to enhance the detection of small particles, and acquisition time was kept constants for all samples, with data collected on a logarithmic scale. Each experiment was performed in four replicates.

10. Staining procedures for Extracted EVs

A 500X stock solution of ExoBrite™ 560/585 cholera toxin subunit B (CTB) EV staining solution (Biotium, San Francisco, USA) was diluted to a final concentration of 50X and added to the precipitated EVs pellet. The solution was gently mixed and incubated for 30 min in the dark at room temperature.

11. Western Blotting

Proteins were extracted using radioimmunoprecipitation assay (RIPA) buffer (Thermo Scientific, Waltham, MA, USA) containing a protease inhibitor cocktail (Thermo Scientific, Waltham, MA, USA). Protein concentrations were determined using the bicinchoninic acid (BCA) assay kit (Thermo Scientific, Waltham, MA, USA). An equal amount of protein (20 μg) was mixed with 5× sodium dodecyl sulfate-polyacrylamide gel electrophoresis (SDS-PAGE) loading buffer (Biosesang, Seongnam, Korea) and heated at 95°C for 10 min. The samples were then separated on a 10% SDS-PAGE gel and transferred to polyvinylidene fluoride (PVDF) membranes (Merck, Darmstadt, Germany). Membranes were blocked

with 5% nonfat skim milk in Tris-buffered saline (10 mM Tris-HCl [pH 7.4] and 0.5 M NaCl) containing 0.1% Tween-20 for 1 h at room temperature. The membranes were then incubated overnight at 4°C with primary antibodies against phospho-p44/42 MAPK (P-ERK) (1:500, Cell Signaling Technology, Danvers, MA, USA), p44/42 MAPK (ERK) (1:500, Cell Signaling Technology, Danvers, MA, USA), phospho-AKT (P-AKT) (1:500, Cell Signaling Technology, Danvers, MA, USA), AKT (1:500, Cell Signaling Technology, Danvers, MA, USA), and GAPDH (1:2000, Santa Cruz, Dallas, TX, USA). The membranes were then incubated with secondary antibodies, goat anti-mouse IgG (H+L) or anti-rabbit IgG (H+L) (1:2000, Thermo Scientific, Waltham, MA, USA), for 1 h at room temperature. Detection was performed using Super Signal West Pico Plus chemiluminescent substrate solution (Thermo Scientific, Waltham, MA, USA), and images were captured using a chemiluminescence imaging system (ImageQuant LAS 4000; General Electric, Chicago, IL, USA). Band intensities were quantified by densitometry using ImageJ software (NIH, Bethesda, Maryland, USA).

12. Assessment of mitochondrial membrane potential

Mitochondrial membrane potential was assessed by confocal microscopy using the fluorescent dye 5′,6,6′-tetrachloro-1,1′,3,3′-tetraethyl benzimidazolyl carbocyanine iodide (JC-1) (Thermo Scientific, Waltham, MA, USA). For JC-1 staining, 1×10^6 cells were incubated with 5 μM JC-1 for 20 min at 37°C in the dark. The cells were then washed once with PBS and analyzed for JC-1

mitochondrial staining using an LSM 980 confocal microscope. Fluorescence intensity was measured at 529 nm (green) and 590 nm (red), and data were quantified and analyzed using ImageJ software.

13. Statistical Analysis

All graphs and statistical analyses were conducted using GraphPad Prism software (GraphPad Software, Inc., San Diego, CA, USA). Data from at least three independent replicates were analyzed and presented as the mean ± SEM. Differences between the control and PS-MPs-treated groups were assessed using one-way analysis of variance (ANOVA). Statistical significance was set at $P < 0.05$, with significance levels indicated as follows: *$P < 0.05$, **$P < 0.01$, and ***$P < 0.001$.

III.RESULTS

1. Cell morphological changes induced by PS-NPs and MPs treatment

To assess the impact of PS-NPs and PS-MPs on cellular structure, ESCs were subjected to 100 nm PS-NPs, 1 μm PS-MPs, and 5 μm PS-MPs for a 24-hour period. The findings indicated that 100 nm PS-NPs and 1 μm PS-MPs led to cell death, while 5 μm PS-MPs did not cause notable structural changes (Figure. 1A). ESCs exposed to 100 nm PS-NPs or 1 μm PS-MPs at 100 μg/mL concentration exhibited significant morphological alterations compared to the control group (Figure. 1B, 1C). In contrast, 5 μm PS-MPs at a higher concentration of 10 mg/mL did not substantially affect cell structure (Figure. 1D).

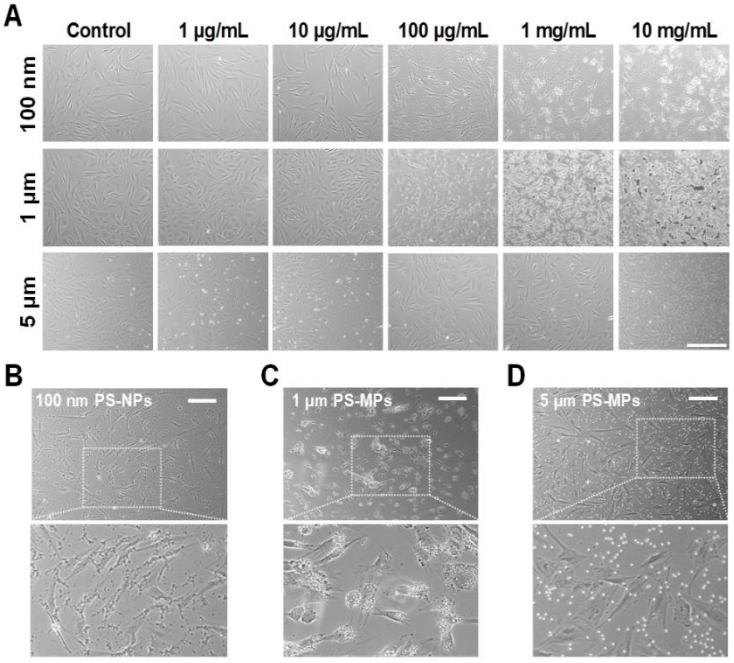

Figure 1. Effect of PS-NPs and MPs treatment concentrations on cellular morphology. (A) ESCs were treated with various concentrations (0 to 10,000 μg/mL) of 100 nm PS-NPs, 1 μm PS-MPs, and 5 μm PS-MPs for 24 h. Scale bar: 50 μm. (B-D) Cell morphology of ESCs treated with 100 nm PS-NPs and 1 μm PS-MPs at a concentration of 100 μg/mL, and with 5 μm PS-MPs at a concentration of 10 mg/mL. Scale bars: 20 μm. PS-NPs, polystyrene nanoplastics; PS-MPs, polystyrene microplastics

2. Cell death induced by 100 nm PS-NPs or 1 μm PS-MPs at 1 mg/mL

When ESCs were treated with PS-NPs or PS-MPs at a concentration of 1 mg/mL, significant changes in cell morphology and a reduction in cell density were observed, except in the case of 5 μm PS-MPs (Figure. 2A). Cell viability in response to different concentrations of PS-NPs and PS-MPs (0 to 10,000 μg/mL) was assessed using the CCK-8 assay. A significant reduction in cell viability was observed after treatment with 100 nm PS-NPs or 1 μm PS-MPs at 1 mg/mL for 24 h, whereas treatment with 5 μm PS-MPs did not affect cell viability (Figure. 2B). These results suggest that the particle size of plastics significantly influences cellular responses, with smaller particles likely to induce greater cellular reactivity.

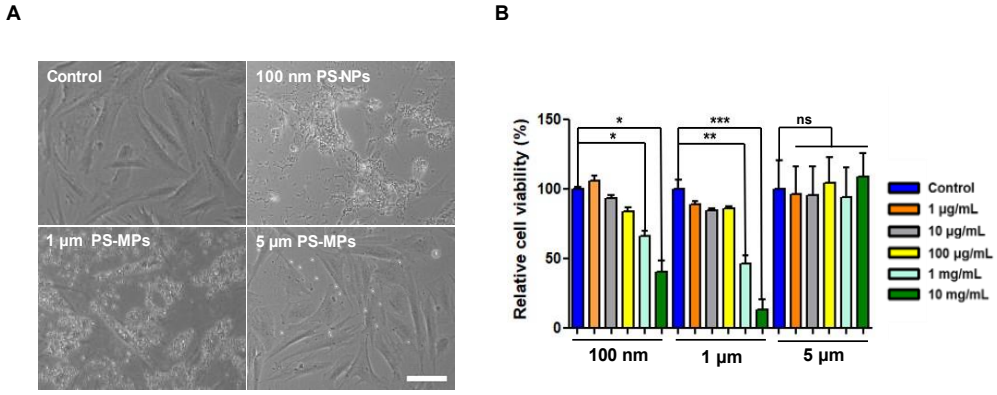

Figure 2. Investigation of cell death based on plastic size and treatment concentrations. (A) Morphological changes in cells treated with 1 mg/mL of 100 nm PS-NPs, 1 μm PS-MPs, and 5 μm PS-MPs. Scale bar: 10 μm. (B) Cell viability as measured by the CCK-8 assay. Data are presented as mean ± SEM and analyzed by Student's t-test. n = 3; significance levels: *P < 0.05, **P < 0.01, ***P < 0.001; ns = not significant.

3. Live-cell imaging of PS-NPs or MPs into a cell

To investigate the cellular entry of PS-NPs and PS-MPs, ESCs treated with 100 nm (FL)PS-NPs or 1 μm (FL)PS-MPs at a concentration of 100 μg/mL were imaged over a 24-hour period using an IncuCyte live-cell imaging system. For ESCs treated with 100 nm (FL)PS-NPs, plastic entry into the nucleus was indicated by an increase in green fluorescence around the nucleus, followed by the appearance of yellow fluorescence within the nucleus over time (Figure. 3A). Similarly, 1 μm (FL)PS-MPs initially exhibited green fluorescence, which transitioned to yellow as they entered the nucleus (Figure. 3B).

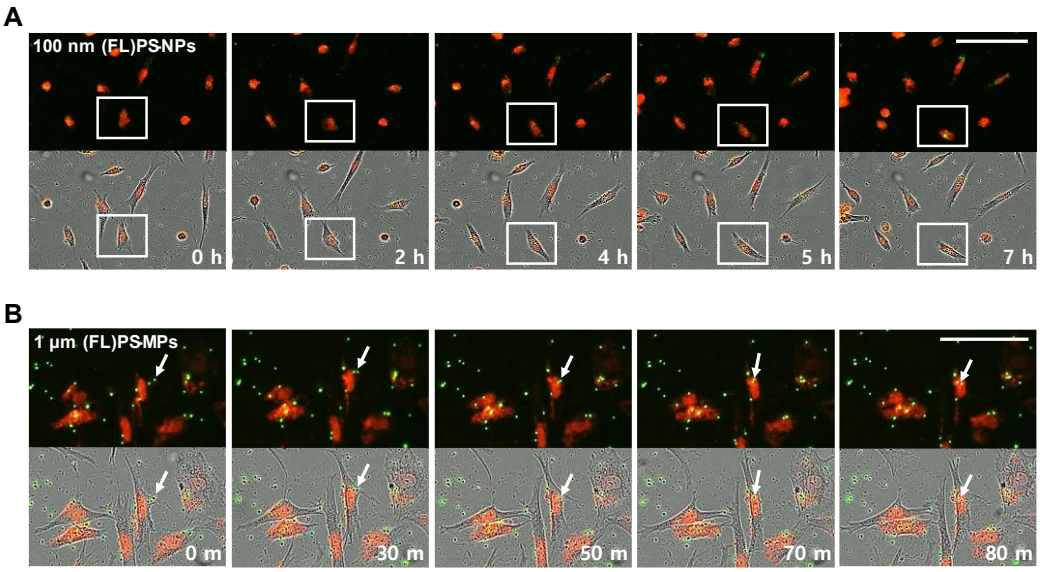

Figure 3. Real-time kinetic data of PS-NPs and MPs nuclear entry using live-cell imaging. (A-B) ESCs were treated with 100 nm fluorescent polystyrene nanoplastics ((FL)PS-NPs) and 1 μm fluorescent polystyrene microplastics ((FL)PS-MPs) for 24 h after nuclear staining with NucSpot 650 (red). Boxes and arrows indicate the entry of 100 nm (FL)PS-NPs and 1 μm (FL)PS-MPs into the nucleus, respectively, as imaged under live conditions using the IncuCyte live imaging system. Scale bar: 100 μm. (FL)PS-NPs, fluorescent polystyrene nanoplastics; (FL)PS-MPs, fluorescent polystyrene microplastics

4. 3D Z-stack imaging reveals nuclear internalization of 100 nm PS-NPs or 1 μm PS-MPs in ESCs

ESCs were treated with 100 nm (FL)PS-NPs or 1 μm (FL)PS-MPs for 24 h. NucSpot Live 650 Nuclear Stain was used to color the nucleus red. Z-stack imaging was employed to visualize the internalization of (FL)PS-NPs and (FL)PS-MPs (Figure. 4). The 3D positioning of particles within cells is illustrated by the ortho XZ plane (yellow box, beneath the 2D image) and the YZ plane (green box, right side of the image) (Figure. 4B & 4E). The 3D z-stack axis of the multiple image overlays (Figure. 4B & 4E) verifies the internalization of 100 nm (FL)PS-NPs and 1 μm (FL)PS-MPs, respectively. The XYZ dimensions show the spatial orientation of (FL)PS-NPs and (FL)PS-MPs in relation to the nucleus. For optimal visualization, the XZ and YZ planes are displayed as vertical sections at the bottom and right of each main XY image in Figure. 4B & 4E.

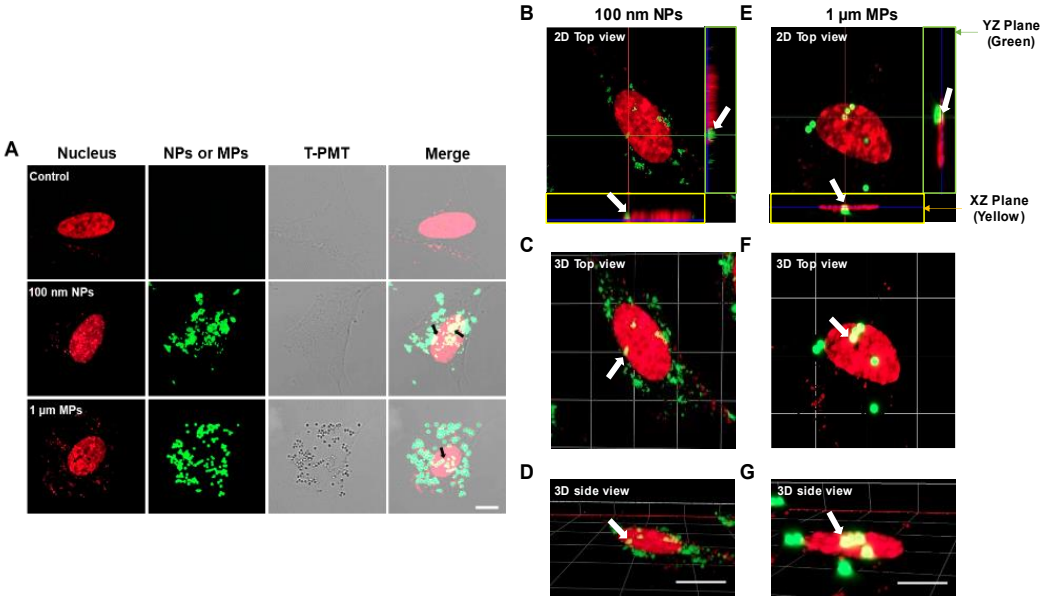

Figure 4. Investigation of plastic cytoplasmic and nuclear accumulation of PS. (A) Representative confocal fluorescence microscopy images showing 100 nm (FL)PS-NPs (green) and 1 μm (FL)PS-MPs (green) in the nucleus (red) and cytoplasm of ESCs cultured under standard conditions. Yellow fluorescence, indicated by arrows, confirms the entry of PS-NPs or PS-MPs into the nucleus. (B-D) Images of ESCs treated with 100 nm (FL)PS-NPs. (E-G) Images of ESCs treated with 1 μm (FL)PS-MPs. Internalization of 100 nm (FL)PS-NPs or 1 μm (FL)PS-MPs is visualized in the Z-axis stacks. Panels (B) and (E) show top-down composite images in a Z-stack. The ortho YZ plane (green box, right in B and E) and the XZ plane (yellow box, bottom in B and E) highlight the internalization of (FL)PS-NPs or PS-MPs within the cells. White arrows indicate the presence of (FL)PS-NPs or PS-MPs. Panels (C) and (F) show 3D top view angles of (B) and (E), respectively, while panels (D) and (G) show 3D side view angles of (B) and (E), respectively. Scale bar: 10 μm.

5. Concentration-dependent distribution of PS-NPs and MPs in the nucleus and cytoplasm of ESCs

The proportion of plastic particles in the cytoplasm and nucleus per cell was measured and depicted in a bar graph. At 1 μg/mL concentration, 100 nm (FL)PS-NPs were detected in 67.8 ± 8.9% of the cytoplasm and 24.8 ± 7.4% of the nucleus. For 1 μm (FL)PS-NPs at 10 μg/mL, 46.2 ± 2.8% were found in the cytoplasm and 6.7 ± 2.9% in the nucleus, while at 100 μg/mL, nearly 97.0 ± 1.3% of particles were observed in the cytoplasm and 42.7 ± 5.2% in the nucleus. These results indicate a concentration-dependent increase in plastic particle entry into both cellular compartments. Notably, treatments exceeding 100 μg/mL resulted in plastic particles being present in almost all cell cytoplasms, with 79.1 ± 8.5% of 100 nm (FL)PS-NPs and 42.7 ± 5.2% of 1 μm (FL)PS-MPs detected in the nucleus compared to the control group (Figure. 5).

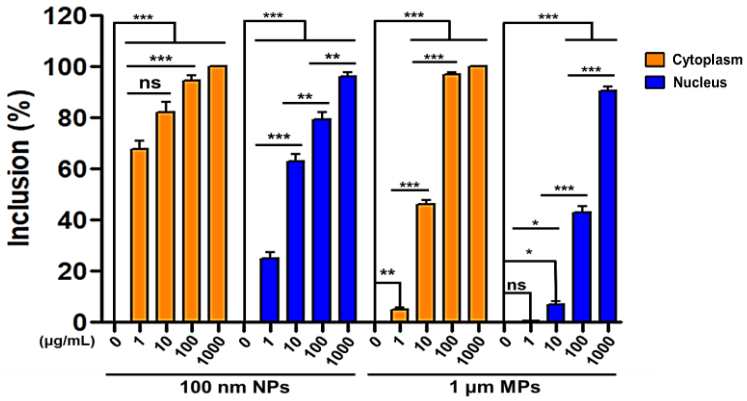

Figure. 5. Size- and concentration-dependent accumulation of plastics in the cytoplasm and nucleus. The number of PS-NPs and PS-MPs present in the cytoplasm and nucleus was quantified and presented as bar graphs. Data are expressed as mean ± SEM and analyzed by Student's t-test. Statistical significance is indicated as follows: *P < 0.05, **P < 0.01, ***P < 0.001; ns = not significant.

6. Release of accumulated PS-NPs and MPs from cells

Using the IncuCyte live-cell imaging system, PS-NPs and PS-MPs that had accumulated in the nucleus were observed to exit the cells (Figure. 6). These findings suggest that plastics accumulated within cells can not only exit and potentially re-enter other cells but can also be transferred between cells by mechanisms involving extracellular vesicles.

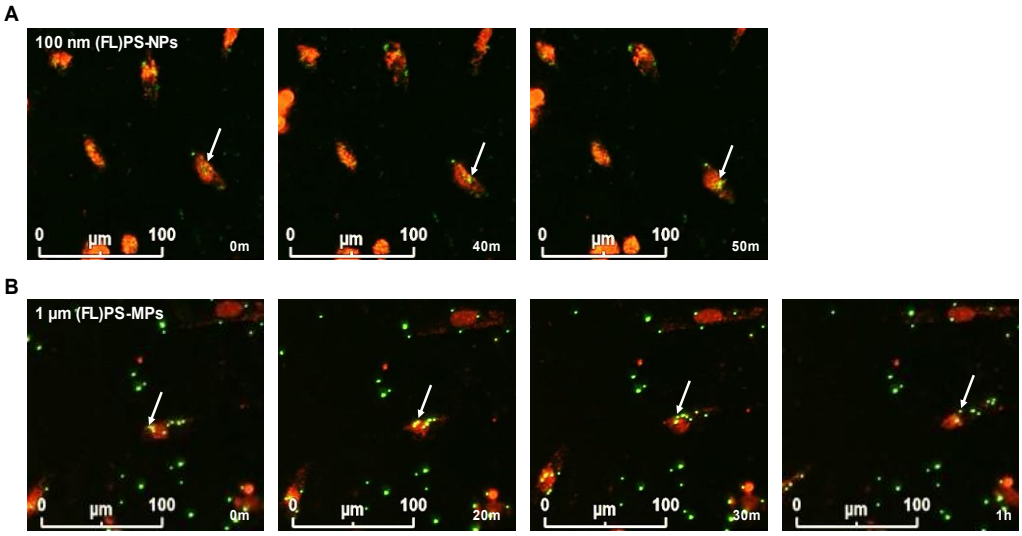

Figure 6. Real-Time analysis of PS-NPs and MPs nuclear entry using live-cell imaging. Cells were treated with 100 nm (FL)PS-NPs or 1 μm (FL)PS-MPs for 24 h, followed by nuclear staining with NucSpot 650 (red). Arrows indicate 100 nm PS-NPs or 1 μm PS-MPs exiting the nucleus after internalization, as observed by live-cell imaging using the IncuCyte Live-Cell Imaging System. Scale bar: 100 μm.

7. Flow cytometry detection of PS-MPs in ESCs

The morphology of subcultured ESCs after treatment with 1 μm PS-MPs and 1 μm (FL)PS-MPs at a concentration of 1 mg/mL is shown in Figure. 7A. Flow cytometric analysis of fluorescence intensity in (FL)PS-MPs-treated cells showed that 47.2 ± 6.8% of the cells in the (FL)PS-MPs treatment group exhibited fluorescence (Figure. 7B & 7C), suggesting internalization of (FL)PS-MPs by the cells.

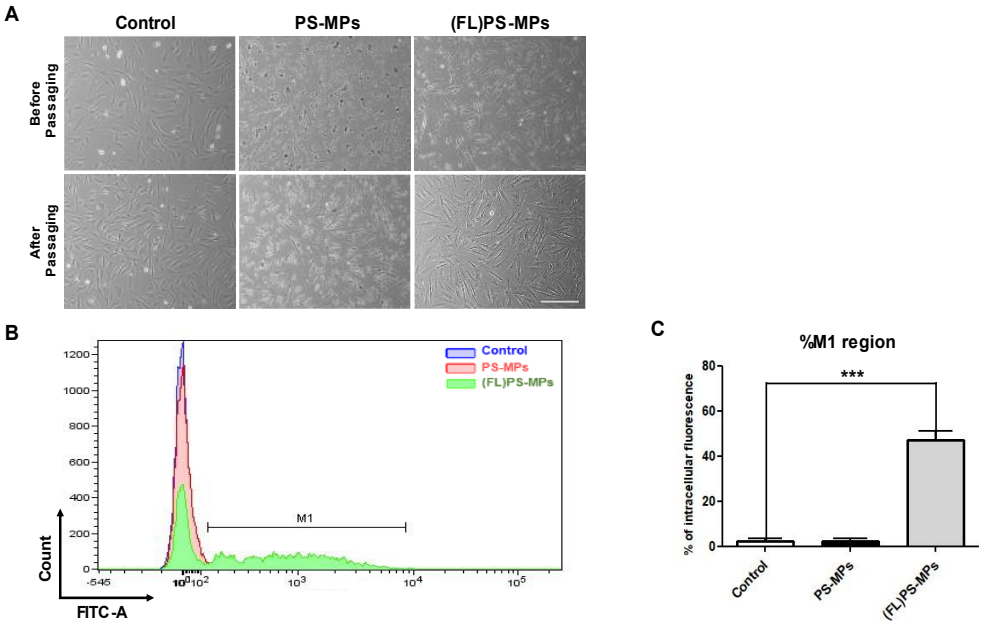

Figure. 7. Detection of intracellular PS-MPs in (FL)PS-MPs-treated ESCs. ESCs were treated with no plastic (control), non-fluorescent 1 μm PS-MPs, or fluorescent (FL)PS-MPs for 24 h followed by passaging. (A) Cell morphology observed 24 h after subculture in response to each treatment. (B) High fluorescence observed in cells treated with (FL)PS-MPs and their subcultured progeny, indicating plastic retention within the cells. The M1 region shows green fluorescence. (C) Percentage of intracellular fluorescence quantified by flow cytometry. Data are presented as mean ± SEM with four biological replicates. Statistically significant difference from control is indicated as ***P < 0.001.

8. Identification of PS-MPs in ESC-derived EVs

To investigate the potential presence of PS-MPs in ESC-derived EVs, extracellular vesicles were extracted from the growth medium of cells exposed to PS-MPs or (FL)PS-MPs and examined for fluorescence using flow cytometry. The findings revealed green fluorescence in EVs from ESCs treated with (FL)PS-MPs (Figure. 8A & 8B), with the fluorescence intensity reaching 51.5 ± 6.5% in (FL)PS-MPs-treated EVs compared to the control group (Figure. 8C). These observations indicate that EVs might contain microplastics and potentially facilitate their transfer between cells.

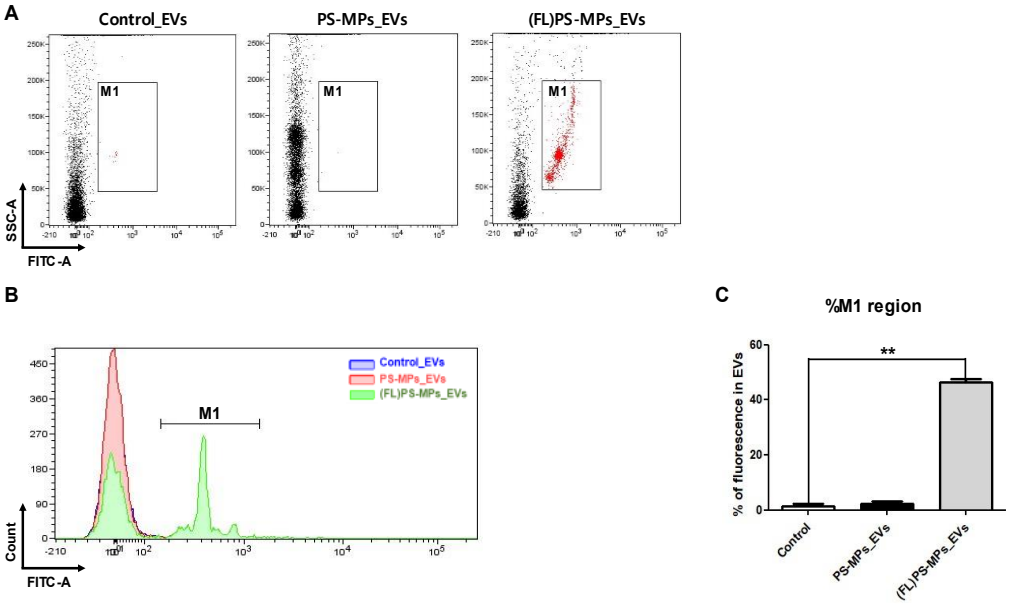

Figure 8. Identification of PS-MPs in ESC-derived EVs. EVs were isolated from the medium of subcultured cells. (A) Flow cytometry plots showing fluorescein isothiocyanate (FITC) versus SSC for EVs. Representative images show changes in dot patterns for PS-MP-treated EVs (PS-MPs_EVs) and green fluorescence in (FL)PS-MPs-treated EVs ((FL)PS-MPs_EVs) compared to the control group. (B) Histogram of EVs with green fluorescence shown and gated in the M1 region, indicating the presence of plastic in (FL)PS-MPs_EVs. (C) Percentage of fluorescence in cell-derived EVs as determined by flow cytometry. Data are presented as mean ± SEM of four biological replicates. A statistically significant difference from the control is indicated as **$P < 0.01$.

9. Flow cytometric detection of PS-MPs in Ishikawa cells

The morphology of subcultured Ishikawa cells after treatment with 1 μm PS-MPs and 1 μm (FL)PS-MPs at a concentration of 1 mg/mL is shown in Figure. 9A. Flow cytometric analysis of fluorescence intensity in (FL)PS-MPs-treated cells revealed that 46.3 ± 8.4% of cells in the (FL)PS-MPs treatment group exhibited fluorescence (Figure. 9B & 9C). These results are consistent with the ESC experiments, indicating that (FL)PS-MPs are internalized by the cells[36].

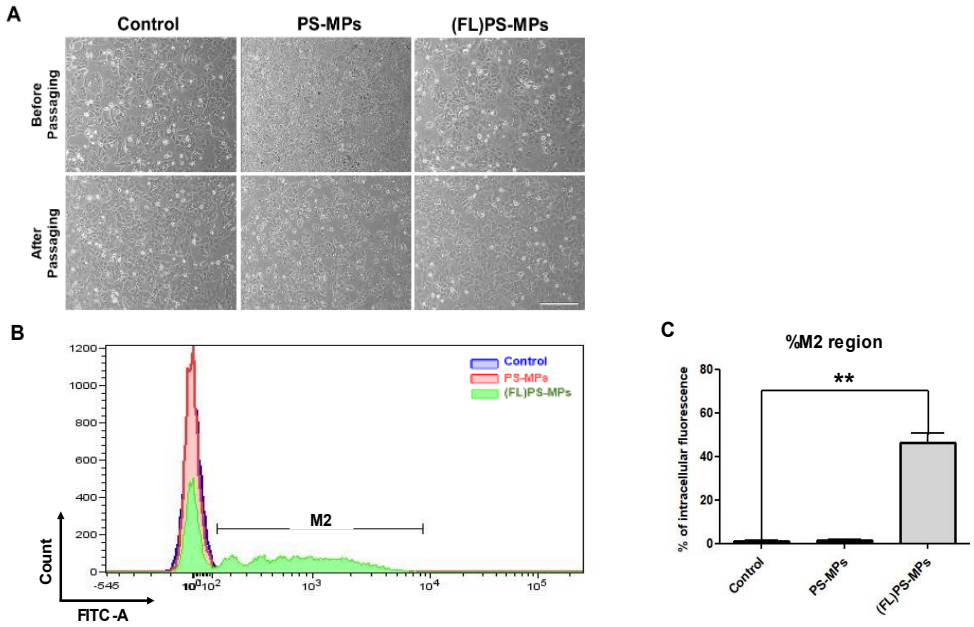

Figure 9. Detection of intracellular PS-MPs in (FL)PS-MPs-treated Ishikawa cells. Ishikawa cells were treated with no plastic (control), non-fluorescent 1 μm PS-MPs, or fluorescent (FL)PS-MPs for 24 h followed by passaging. (A) Cell morphology observed 24 h after subculture in response to each treatment. (B) High fluorescence observed in cells treated with (FL)PS-MPs and their subcultured progeny, indicating plastic retention within the cells. The M2 region shows green fluorescence. (C) Percentage of intracellular fluorescence quantified by flow cytometry. Data are presented as mean ± SEM with four biological replicates. A statistically significant difference from the control group is indicated as $^{**}P < 0.01$.

10. Identification of PS-MPs in Ishikawa cell-derived EVs

To evaluate the presence of PS-MPs in EVs derived from Ishikawa cells, EVs were isolated from the culture medium of cells treated with PS-MPs or (FL)PS-MPs and analyzed for fluorescence by flow cytometry. The results showed green fluorescence in EVs from (FL)PS-MPs-treated Ishikawa cells (Figure. 10A & 10B), with the fluorescence intensity reaching 51.6 ± 6.2% in (FL)PS-MPs_EVs compared to the control group (Figure. 10C). These results suggest that EVs can deliver MPs and facilitate cell-to-cell migration, which is consistent with the results from ESCs experiments [36].

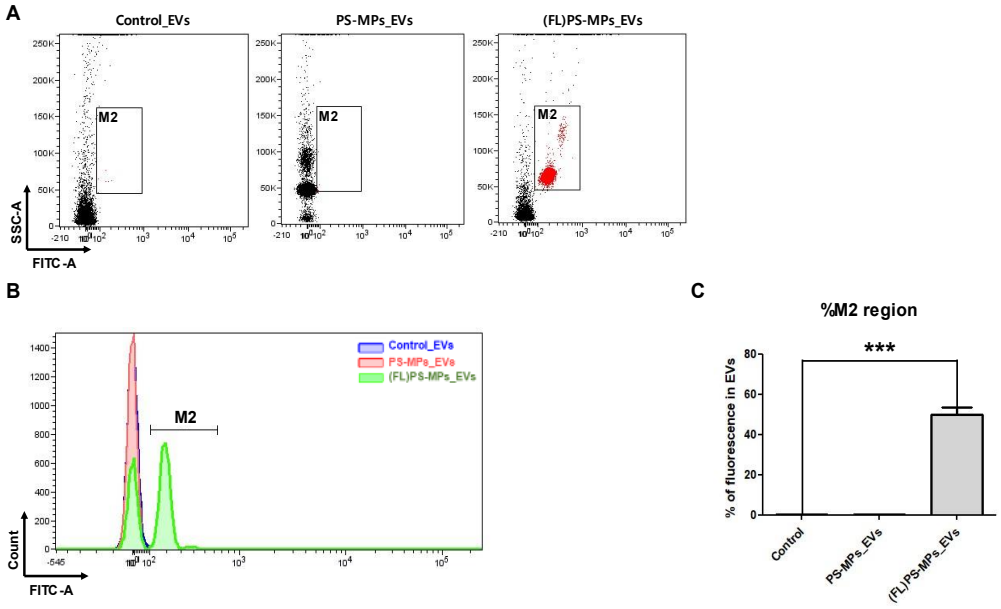

Figure. 10. Detection of PS-MPs in EVs derived from Ishikawa cells. (A) Flow cytometry plots of fluorescein isothiocyanate (FITC) versus SSC for EVs, showing representative images of dot pattern changes in PS-MPs_EVs and green fluorescence in (FL)PS-MPs_EVs compared to the control group. (B) Histogram of EVs with green fluorescence shown and gated in the M2 region, indicating the presence of plastic in (FL)PS-MPs_EVs. (C) Percentage of fluorescence in cell-derived EVs as determined by flow cytometry. Data are presented as mean ± SEM of four biological replicates. Statistically significant difference from control is indicated as ***P < 0.001.

11. Identification of PS-MPs in stained EVs derived from Ishikawa cells

To further confirm the presence of plastics in EVs, extracted EVs membranes were stained, and fluorescence intensity was analyzed by flow cytometry. The results showed that EVs membranes from the control group showed only red fluorescence (Figure. 11A-1 & A-2), whereas EVs membranes from the (FL)PS-MPs treatment group showed both green and red fluorescence (Figure. 11B-1 & B-2). These results suggest the presence of MPs in EVs[36].

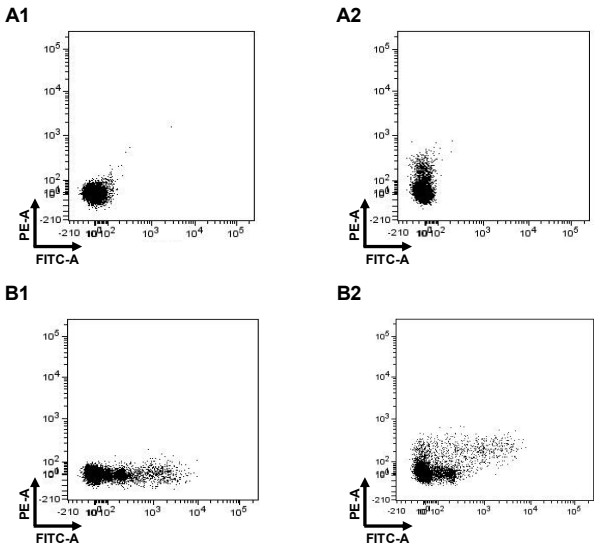

Figure. 11. Visualization of PS-MPs in EVs stained and derived from Ishikawa cells. Control EVs showed a shift in the dot pattern when stained (A2) compared to the unstained condition (A1), confirming the staining of the EVs. Similarly, (FL)PS-MPs_EVs showed a change in dot pattern when stained (B2) compared to unstained (B1), indicating the presence of microplastics within the stained EVs.

12. Visualization of PS-MPs intracellular accumulation after EVs treatment

To study the entry of EV-derived PS-MPs into cells, cells were treated with stained (FL)PS-MPs_EVs and imaged over 24 h using the IncuCyte live-cell imaging system. After treatment, vesicles containing PS-MPs, visible as yellow signals, gradually fused with the cells at approximately 6 h and 50 min, with microplastics ultimately observed inside the cells (Figure. 12). These results suggest that EVs facilitate cell-to-cell transfer of PS-MPs[36].

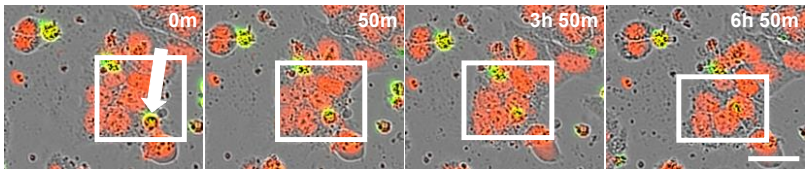

Figure. 12. Live-Cell Imaging of PS-MPs entry into cells mediated by cell-derived EVs in real-time. (FL)PS-MPs_EVs stained with ExoBrite solution (red) were applied to Ishikawa cells with nuclei stained with NucSpot 650 (red) for 24 h. Yellow fluorescence (indicated by arrows) indicates the presence of (FL)PS-MPs (green) within the EVs. (FL)PS-MPs contained in EVs entering cells (indicated by boxes) were observed in live-cell imaging using the IncuCyte system. Scale bar = 30 μm.

13. Analysis of PS-MPs intracellular accumulation after EVs treatment

To examine the cellular uptake of PS-MPs delivered by EVs, researchers exposed cells to EVs for 24 hours and utilized confocal microscopy to detect PS-MPs. The findings revealed that cells treated with EVs from PS-MP-exposed cells contained detectable PS-MPs (Figure. 13A). Z-stack imaging confirmed the presence of PS-MPs inside the cells (Figure. 13B). A yellow box at the top of the 2D image highlights the ortho XZ plane, while a green box on the right shows the YZ plane (Figure. 13B-1). The 3D Z-stack axis in Figure. 13B-1 displays internalized PS-MPs, with their location relative to the red-stained nucleus determined from XYZ dimensions. In Figure. 13B-1, vertical sections of the XZ and YZ planes are presented at the bottom and right of each main XY image for optimal visualization. These observations suggest that MPs can be transported intracellularly via EVs [36].

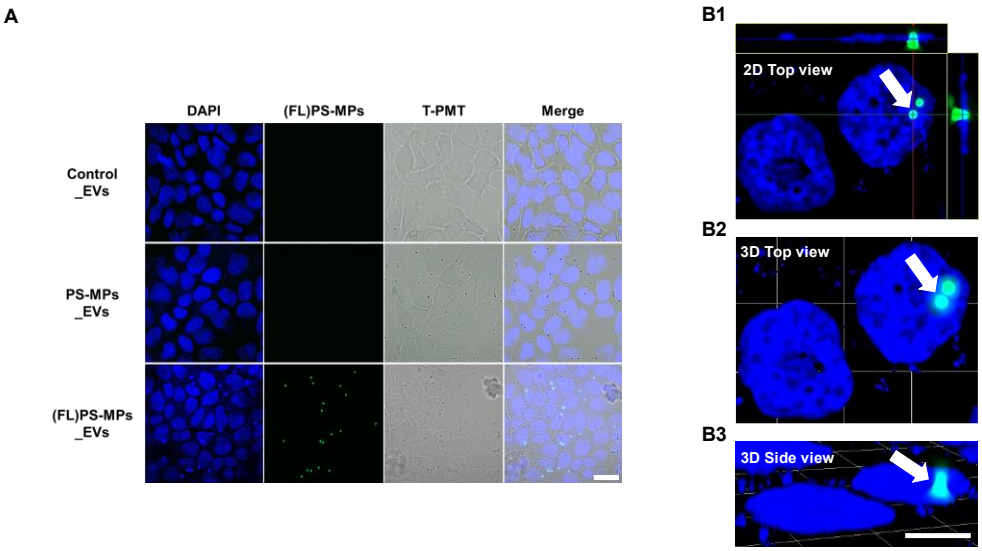

Figure. 13. Analysis of PS-MPs intracellular accumulation after exposure to cell-derived EVs. (A) Confocal microscopy images depict Ishikawa cells cultured under normal conditions after 24-hour treatment with cell-derived EVs. Scale bars = 20 μm. (B) Images of (FL)PS-MP_EV-treated cultures demonstrate internalization of 1 μm PS-MPs within the z-stack axis. (B1) Top-down merge of the Z-stack image. PS-MP internalization is visible in the ortho YZ plane (green border, right panel of B1) and XZ plane (yellow border, upper panel of B1). White arrows indicate MPs within cells. (B2) 3D top view of (B1). (B3) 3D side view of (B1). Scale bars = 10 μm.

14. PS-NPs decrease ESCs proliferation and induce apoptosis

To investigate cell proliferation in ESCs treated with 100 nm PS-NPs or 1 μm PS-MPs, we examined the expression of P-AKT, AKT, P-ERK, and ERK by Western blot. A reduction in proliferation was observed in cells treated with 100 μg/mL of 100 nm PS-NPs, as indicated by a decreased P-AKT/AKT and P-ERK/ERK ratio compared to the control. In contrast, treatment with 1 μm PS-MPs showed no significant effect (Figure. 5A & 5B).

To assess cell apoptosis, we performed JC-1 staining to evaluate mitochondrial membrane potential. JC-1, a potentiometric dye, shifts fluorescence emission from red to green as JC-1 aggregates (indicating polarized mitochondria) transition to monomers (depolarized mitochondria), with mitochondrial depolarization represented by a decrease in the aggregate/monomer fluorescence intensity ratio. JC-1 mitochondrial staining patterns in all experimental groups were visualized by confocal microscopy (Figure. 5C), showing a decrease in the aggregate/monomer ratio in both 100 nm PS-NP and 1 μm PS-MPs treatments compared to the control. However, only the 100 nm PS-NP treatment induced significant apoptosis (Figure. 5D).

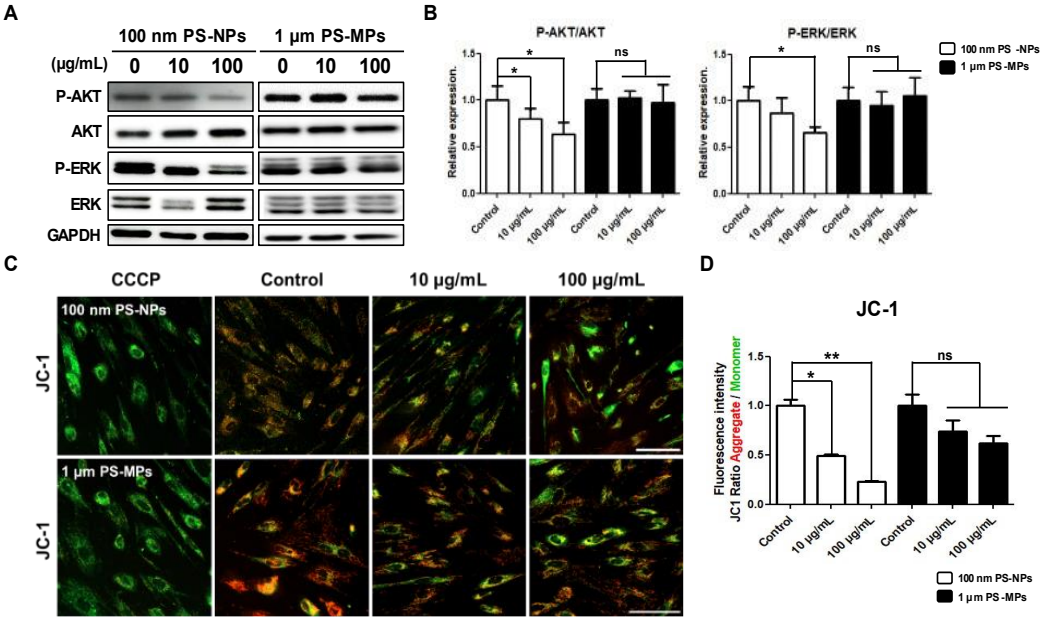

Figure. 14 Analysis of proliferation marker and apoptosis cells treated with PS-NPs or MPs. (A) Representative Western blot bands showing protein expression of proliferation markers (P-AKT, AKT, P-ERK, ERK) in ESCs treated with 100 nm PS-NPs or 1 μm PS-MPs. (B) P-AKT/AKT and P-ERK/ERK ratios were calculated using GAPDH as an internal control. Data are expressed as mean ± SEM; n = 7 for 100 nm PS-NPs, n = 4 for 1 μm PS-MPs. $P < 0.05$ vs. control; ns = not significant. (C) ESCs were exposed to 100 nm PS-NPs, 1 μm PS-MPs or CCCP (positive control) for 24 h and depolarization of mitochondrial membrane potential was observed. Scale bar: 100 μm. (D) Quantitative analysis of aggregate/monomer fluorescence intensity ratio. Red and green fluorescence results are superimposed and expressed as mean ± SEM of triplicate samples. Data were analyzed by Student's t-test (n = 3); significance indicated as *$P < 0.05$, **$P < 0.01$ vs. control; ns = not significant.

IV. DISCUSSION

This research employed real-time imaging to observe PS-NP and MP entry into cells. Both 100 nm PS-NPs and 1 μm PS-MPs caused notable changes in cell morphology and viability, effects not seen with 5 μm PS-MPs. Confocal microscopy was used to closely examine intracellular accumulation of PS-NPs and MPs, particularly in the nuclei. The researchers quantitatively assessed the ratios of PS-NP and MP accumulation in the nucleus and cytoplasm, correlating these with particle size and concentration. Additionally, they investigated cell-to-cell transfer of PS-MPs via EVs. To verify PS-MP presence within EVs, fluorescently labeled (FL)PS-MPs and EV staining were used, with double staining confirmed by flow cytometry. The double-stained (FL)PS-MPs_EVs were then introduced to cells, enabling real-time tracking of PS-MP entry via EVs.

Earlier studies have demonstrated that plastics can penetrate cell membranes and induce morphological changes. In vitro research on human liver and kidney cells indicated that MPs form clusters in a ring-like pattern around nuclei after cytoplasmic penetration, affecting cell morphology, metabolism, proliferation, and cellular stress [30]. Moreover, treatment of human gastric cells with NPs or MPs has been shown to increase cellular stress and trigger apoptosis-necrosis [31]. This study builds upon these findings by investigating plastic particle accumulation in the

cytoplasm and nucleus of ESCs, with a focus on particle size and concentration. Furthermore, the researchers examined proliferation markers and apoptotic changes in cells treated with 100 nm PS-NPs or 1 μm PS-MPs.

The significance of ESCs stems from the crucial role the human endometrium plays in embryo implantation and fertility. Animal studies using rodents have demonstrated that MPs can cause ovarian fibrosis and apoptosis in granulosa cells [32]. Furthermore, both NPs and MPs have been found to elevate ROS and inflammation in oocytes, resulting in diminished oocyte quality, thinning of the endometrium, and ovarian inflammation, all of which could impact pregnancy outcomes [20,27]. Despite these findings, research on plastic accumulation in the human endometrium and its effects on ESCs remains limited. Our research revealed that 100 nm PS-NPs accumulated more effectively in ESCs compared to 1 μm PS-MPs, even at lower concentrations, and caused a more significant decrease in cell proliferation and increase in apoptosis. These findings align with other studies suggesting that smaller plastic particles are more easily internalized by cells or organisms. The impact of these particles on cellular function appears to be influenced by their size, dose, and characteristics, as well as the specific cell line exposed [30,33-34].

A key advantage of this study is the utilization of real-time imaging with

fluorescently labeled plastics, enabling kinetic analysis of plastic accumulation in ESCs. By employing confocal microscopy and the IncuCyte system, we were able to differentiate between plastic internalization and surface deposition by monitoring the temporal progression of fluorescence. The transition from green fluorescence surrounding the nucleus to yellow fluorescence within the nucleus confirmed internalization. This approach offers valuable insights into the molecular interactions between endometrial cells and plastic particles.

The small size of 100 nm PS-NPs made direct visualization of their entry into cells challenging. However, high-magnification confocal microscopy and 3D z-stack analysis allowed for precise observation of plastic accumulation in the cytoplasm and nucleus. XYZ spatial analysis revealed distinct internalization patterns (Figure. 4B-G), while quantitative bar graph analysis (Figure. 5) confirmed size- and concentration-dependent accumulation within cellular compartments. These results indicate that plastic particles penetrate the cell membrane and accumulate in the nucleus, potentially inducing molecular changes. Notably, previous studies have shown that smaller plastic particles exert stronger effects on cells, and our results support this finding, as 100 nm PS-NPs induced a more pronounced decrease in cell proliferation and increased apoptosis compared to 1 μm PS-NPs (Figure. 14). These findings suggest that NPs may have a more

detrimental effect on endometrial stromal cells than MPs, potentially contributing to endometrial-related diseases.

Recent research indicates that MPs are involved in the production and transformation of EVs in cells. Wang et al. observed a 4.3-fold increase in EVs production in cells treated with PS-MPs compared to untreated cells [26]. Additionally, the size of EVs varied according to the concentration of MPs, suggesting that MPs not only stimulate increased EVs production but also influence variations in EVs size. Studies have reported that miRNAs within EVs, whose expression is altered by exposure to MPs, are associated with the development of metabolic syndrome and diabetes[25,27]. While recent research has highlighted the effects of altered EV expression, there remains a limited understanding of the mechanisms by which accumulated MPs are transferred to other organs.

Mierzejewski et al. demonstrated that PET-MPs are transported in serum-derived EVs in an immature gilt model, with results indicating that PET-MPs negatively impact physical function through differentially regulated miRNAs. This study suggests that MPs are not only transported by EVs but may also migrate to other organs. In our study, we observed the migration of intracellularly accumulated PS-MPs out of the cell (Figure. 6), suggesting that EVs facilitate the transfer of MPs to other cells and tissues. These results provide clear evidence for the mechanism of

cell-to-cell transfer of PS-MPs via EVs.

To minimize residual PS-MPs when extracting EVs from MPs-treated cells, cells were treated with PS-MPs for 24 h, washed three times, and then EVs were isolated from the medium of the passaged cells. The experiments were first verified using ESCs as primary cells (Figure. 7 & 8) and then repeated using Ishikawa cells as a cell line (Figure. 9 & 10). To confirm whether PS-MPs were present within cell-derived EVs or merely aggregated, EVs were stained and observed using the IncuCyte live cell imaging system to detect color-merged vesicles. The temporal sequence of images showed yellow vesicles surrounding and gradually fusing with the cell, resulting in intracellular accumulation of microplastics, indicating that PS-MPs within the EVs were internalized by the cell (Figure. 12). Although the low magnification of the IncuCyte system limited close observation of PS-MPs internalization, the 3D z-stack capability of confocal microscopy allowed precise visualization of PS-MPs internalization within cells (Figure. 13).

Studies have shown that MPs affect the size of EVs, suggesting that accumulation of MPs in EVs may contribute to size variation. Our findings highlight the need for further research to assess the cytotoxicity of MPs at the cellular level and to explore the effects of EV-delivered MPs on cells, particularly in relation to the potential development of endometrial-related diseases.

V. CONCLUSION

Our investigation revealed that the size and concentration of plastic particles are critical factors in determining the cellular response of ESCs. This study is the first to visualize plastic entry into ESCs using real-time imaging, providing a comprehensive understanding of the dynamic interactions between plastics and cells. In addition, we examined proliferation pathways and apoptotic changes in cells exposed to 100 nm PS-NPs or 1 μm PS-MPs, demonstrating that PS-NPs may negatively impact human endometrial health. Furthermore, our results showed that PS-MPs can be transferred between cells via cell-derived EVs. Supported by real-time imaging and detailed analysis, these findings contribute to the understanding of the dynamics of EV-derived PS-MPs internalization into cells.

Our findings highlight the need for further research into the potential effects of plastics on human endometrial stromal cells and the broader health implications of plastic-containing EVs in humans. These findings advance our knowledge of the mechanisms underlying the adverse effects of plastics on reproductive health, particularly with regard to endometrial disease and infertility.

REFERENCES

1. Aslani H, Pashmtab P, Shaghaghi A, Mohammadpoorasl A, Taghipour H, Zarei M. Tendencies towards bottled drinking water consumption: Challenges ahead of polyethylene terephthalate (PET) waste management. Health Promot Perspect. 2021;11(1):60-8. doi: 10.34172/hpp.2021.09.
2. Tiseo I. Global plastic production 1950–2020. Statista, September. 2021;20.
3. Horton AA, Walton A, Spurgeon DJ, Lahive E, Svendsen C. Microplastics in freshwater and terrestrial environments: Evaluating the current understanding to identify the knowledge gaps and future research priorities. Sci Total Environ. 2017; 586:127-41. Epub 20170204. doi: 10.1016/j.scitotenv.2017.01.190. PubMed PMID: 28169032.
4. MacLeod M, Arp HPH, Tekman MB, Jahnke A. The global threat from plastic pollution. Science. 2021;373(6550):61-5. doi: 10.1126/science. abg5433. PubMed PMID: 34210878.
5. Zhu J, Wang J, Chen R, Feng Q, Zhan X. Cellular Process of Polystyrene Nanoparticles Entry into Wheat Roots. Environmental Science & Technology. 2022;56(10):6436-44. doi: 10.1021/acs.est.1c08503.
6. O'Brine T, Thompson RC. Degradation of plastic carrier bags in the marine environment. Mar Pollut Bull. 2010;60(12):2279-83. Epub 20101018. doi: 10.1016/j.marpolbul.2010.08.005. PubMed PMID: 20961585.
7. Liu Z, You X-y. Recent progress of microplastic toxicity on human exposure base on in vitro and in vivo studies. Science of The Total Environment. 2023; 903:166766.
8. Akdogan Z, Guven B, Kideys AE. Microplastic distribution in the surface water and sediment of the Ergene River. Environmental Research. 2023; 234:116500.
9. Wei Z, Wang Y, Wang S, Xie J, Han Q, Chen M. Comparing the effects of polystyrene microplastics exposure on reproduction and fertility in male and female mice. Toxicology. 2022; 465:153059. Epub 20211202. doi: 10.1016/j.tox.2021.153059. PubMed PMID: 34864092.
10. Huang J, Zou L, Bao M, Feng Q, Xia W, Zhu C. Toxicity of polystyrene nanoparticles for mouse ovary and cultured human granulosa cells. Ecotoxicol Environ Saf. 2023; 249:114371. Epub 20221209. doi: 10. 1016/j.ecoenv.2022.114371. PubMed PMID: 36508839.
11. Yang D, Zhu J, Zhou X, Pan D, Nan S, Yin R, et al. Polystyrene micro- and nano-particle coexposure injures fetal thalamus by inducing ROS-mediated cell apoptosis. Environ Int. 2022; 166:107362. Epub 20220618. doi: 10.1016/j.envint.2022.107362. PubMed PMID: 35749991.
12. Chae Y, Kim D, Kim SW, An YJ. Trophic transfer and individual impact of nano-sized polystyrene in a four-species freshwater food chain. Sci Rep. 2018;8(1):284. Epub 20180110. doi: 10.1038/s41598-017-18849-y. PubMed PMID: 29321604; PubMed Central PMCID: PMCPMC5762726.
13. Yuan Z, Nag R, Cummins E. Human health concerns regarding microplastics in the aquatic environment - From marine to food systems. Science of The Total Environment. 2022; 823:153730.
14. Qin X, Cao M, Peng T, Shan H, Lian W, Yu Y, et al. Features, Potential Invasion Pathways, and Reproductive Health Risks of Microplastics Detected in Human Uterus. Environmental Science & Technology. 2024;58(24):10482-93. doi: 10.1021/acs.est.4c01541.
15. Haddadi A, Kessabi K, Boughammoura S, Rhouma MB, Mlouka R, Banni M, et al. Exposure to microplastics leads to a defective ovarian function and change in cytoskeleton protein expression in rat. Environ Sci Pollut Res Int. 2022;29(23):34594-606. Epub 20220118. doi: 10.1007/s11356-021-18218-3. PubMed PMID: 35040070.
16. Wu H, Xu T, Chen T, Liu J, Xu S. Oxidative stress mediated by the TLR4/NOX2 signalling

axis is involved in polystyrene microplastic-induced uterine fibrosis in mice. Science of the Total Environment. 2022;838(Part 2):155825. PubMed PMID: S0048969722029229.
17. Hao S, Yang H, Hu J, Luo L, Yuan Y, Liu L. Bioactive compounds and biological functions of medicinal plant-derived extracellular vesicles. Pharmacol Res. 2024:107062. Epub 20240109. doi: 10.1016/j.phrs.2024.107062. PubMed PMID: 38211637.
18. Sarkar S, Patranabis S. Emerging Role of Extracellular Vesicles in Intercellular Communication in the Brain: Implications for Neurodegenerative Diseases and Therapeutics. Cell Biochem Biophys. 2024. Epub 20240201. doi: 10.1007/s12013-024-01221-z. PubMed PMID: 38300375.
19. Doyle LM, Wang MZ. Overview of extracellular vesicles, their origin, composition, purpose, and methods for exosome isolation and analysis. Cells. 2019;8(7):727.
20. Reseco L, Molina-Crespo A, Atienza M, Gonzalez E, Falcon-Perez JM, Cantero JL. Characterization of Extracellular Vesicles from Human Saliva: Effects of Age and Isolation Techniques. Cells. 2024;13(1). Epub 20240102. doi: 10.3390/cells13010095. PubMed PMID: 38201299; PubMed Central PMCID: PMCPMC10778510.
21. Wang Y, Cai S, Chen X, Sun Q, Yin T, Diao L. The role of extracellular vesicles from placenta and endometrium in pregnancy: Insights from tumor biology. Journal of Reproductive Immunology. 2024; 162:104210.
22. Mierzejewski K, Kurzyńska A, Golubska M, Całka J, Gałęcka I, Szabelski M, et al. New insights into the potential effects of PET microplastics on organisms via extracellular vesicle-mediated communication. Science of The Total Environment. 2023; 904:166967.
23. Wang Y-L, Huang CC-Y, Zheng C-M, Liu W-C, Lee Y-H, Chiu H-W. Polystyrene microplastic-induced extracellular vesicles cause kidney-related effects in the crosstalk between tubular cells and fibroblasts. Ecotoxicology and Environmental Safety. 2024; 273:116098.
24. Thoma ME, McLain AC, Louis JF, King RB, Trumble AC, Sundaram R, et al. Prevalence of infertility in the United States as estimated by the current duration approach and a traditional constructed approach. Fertility and Sterility. 2013;99(5):1324-31. e1.
25. Inhorn MC, Patrizio P. Infertility around the globe: new thinking on gender, reproductive technologies and global movements in the 21st century. Hum Reprod Update. 2015;21(4):411-26. Epub 20150322. doi: 10.1093/humupd/dmv016. PubMed PMID: 25801630.
26. Unuane. D, Poppe. K. Female infertility: do we forget the thyroid? Journal of Endocrinological Investigation: Official Journal of Italian Society of Endocrinology (SIE). 2015;38(5):571. PubMed PMID: edssjs. FCD5851F.
27. Revel A. Multitasking human endometrium: a review of endometrial biopsy as a diagnostic tool, therapeutic applications, and a source of adult stem cells. Obstet Gynecol Surv. 2009;64(4):249-57. doi: 10.1097/OGX.0b013e318195136f. PubMed PMID: 19296860.
28. J. S, M. S, T. W, X. T, J. S, M. C. Detection and quantification of various microplastics in human endometrium based on laser direct infrared spectroscopy. Science of the Total Environment. 2024; 906:167760. PubMed PMID: edselc.2-52.0-85173832768.
29. Salvioli S, Ardizzoni A, Franceschi C, Cossarizza A. JC-1, but not DiOC6(3) or rhodamine 123, is a reliable fluorescent probe to assess delta psi changes in intact cells: implications for studies on mitochondrial functionality during apoptosis. FEBS Lett. 1997;411(1):77-82. doi: 10.1016/s0014-5793(97)00669-8. PubMed PMID: 9247146.
30. Goodman KE, Hua T, Sang QA. Effects of Polystyrene Microplastics on Human Kidney and Liver Cell Morphology, Cellular Proliferation, and Metabolism. ACS Omega. 2022;7(38):34136-53. Epub 20220919. doi: 10.1021/acsomega.2c03453. PubMed PMID: 36188270; PubMed Central PMCID: PMCPMC9520709.

31. Banerjee A, Billey LO, Shelver WL. Uptake and toxicity of polystyrene micro/nanoplastics in gastric cells: Effects of particle size and surface functionalization. PLoS One. 2021;16(12): e0260803. Epub 20211231. doi: 10.1371/journal.pone.0260803. PubMed PMID: 34971556; PubMed Central PMCID: PMCPMC8719689.
32. R. A, X. W, L. Y, J. Z, N. W, F. X, et al. Polystyrene microplastics cause granulosa cells apoptosis and fibrosis in ovary through oxidative stress in rats. Toxicology. 2021; 449:152665.
33. Yang Z, Wang M, Feng Z, Wang Z, Lv M, Chang J, et al. Human Microplastics Exposure and Potential Health Risks to Target Organs by Different Routes: A Review. Current Pollution Reports. 2023;9(3):468-85. doi: 10.1007/s40726-023-00273-8.
34. Kumar N, Lamba M, Pachar AK, Yadav S, Acharya A. Microplastics – A Growing Concern as Carcinogens in Cancer Etiology: Emphasis on Biochemical and Molecular Mechanisms. Cell Biochemistry and Biophysics. 2024. doi: 10.1007/s12013-024-01436-0.
35. Płuciennik K, Sicińska P, Misztal W, Bukowska B. Important Factors Affecting Induction of Cell Death, Oxidative Stress and DNA Damage by Nano- and Microplastic Particles In Vitro. Cells. 2024;13(9). Epub 20240430. doi: 10.3390/cells13090768. PubMed PMID: 38727304; PubMed Central PMCID: PMCPMC11083305.
36. Kim N, Park JH, Lee I, Jung GS, Lee JH, Lee MJ, et al. Investigation of cell-to-cell transfer of polystyrene microplastics through extracellular vesicle-mediated communication. Biochemical and Biophysical Research Communications. 2024;734:150719.
37. Nara Kim, Joo Hyun Park, Gee Soo Jung et al. Investigation of potential detrimental effects of nano- and microplastics in human endometrial stromal cells, 11 April 2024, PREPRINT (Version 1) available at Research Square [https://doi.org/10.21203/rs.3.rs-4210827/v1]

ABSTRACT (IN KOREAN)

논문제목

미세 플라스틱이 인간 자궁 내막 세포에 미치는 영향 조사 및 세포 간 이동

<지도교수 조 시 현>

연세대학교 대학원 의료기기산업학과

김나라

최근 몇 년 동안 나노플라스틱(Nanoplastics: NPs)과 미세플라스틱(MPs)은 전 세계적인 관심사가 되었습니다. 그러나 폴리스티렌(PS)-NPs와 MPs가 여성의 자궁내막에 미치는 영향은 아직 명확히 밝혀지지 않았습니다. 따라서 본 연구에서는 인간 자궁내막 기질세포(ESCs)에 다양한 플라스틱 크기와 농도를 사용하여 PS-NPs와 MPs에 대한 적절한 시험관 내 노출 프로토콜을 확립하고, ESCs에 대한 PS-NP와 MPs의 세포 독성 영향과 MPs의 세포 간 전이 가능성을 조사하고자 했습니다. 특히 100 nm PS-NPs와 1㎛ PS-MPs와 같은 작은 플라스틱은 5㎛ PS-MPs와 같은 큰 플라스틱에 비해 세포 흡수 경향이 더 높은 것으로 나타났습니다. 이러한 작은 플라스틱 입자는 24시간 동안 100㎍/mL를 초과하는 농도에서 눈에 띄는 세포의 형태학적 변화를 유도하고, 세포 사멸을 유발하는 것을 보였습니다. 또한, 공초점 현미경과 실시간 이미징 장치를 사용하여 플라스틱 입자가 ESCs의 핵과 세포질에 축적될 뿐만 아니라 다양한 세

포 유형에 의해 환경으로 방출되고, 세포 간 단백질, 핵산 및 지질의 교환을 통해 세포 간 및 세포 내 통신에 크게 관여하는 지질 이중층으로 둘러싸인 작은 막 입자인 세포 외 소포체(EVs)를 통해 MPs가 세포간 이동한다는 사실도 확인했습니다. 더 나아가 플라스틱의 크기와, 핵과 세포질에 침투하는 정도 사이에 뚜렷한 상관관계가 있는 것을 확인한 결과 플라스틱의 크기가 작을수록 세포내 플라스틱의 내재화 비율이 상당히 높은 것으로 나타났습니다. 또한, 100nm PS-NPs로 세포를 처리했을 때, 1㎛ PS-MPs를 처리했을 때와 달리 ESCs의 증식이 감소하고 세포 사멸이 유도되는 것을 확인함으로써 플라스틱의 사이즈가 작을수록 ESCs에 더 부정적인 영향을 끼칠 수 있음을 확인하였습니다. 결론적으로, 이 연구는 100nm PS-NPs와 1㎛ PS-MPs에 노출되면 ESCs 내에 이러한 입자가 동적으로 축적되어 특정 농도에서 세포 사멸 또는 증식 감소로 이어진다는 사실을 입증한 최초의 연구입니다. 이번 연구 결과는 이러한 입자가 생식 능력과 생식 건강에 잠재적으로 악영향을 미칠 수 있음을 시사하며, 정확한 분자 메커니즘을 밝히기 위한 추가 연구의 필요성을 강조합니다.

핵심 되는 말: 미세 플라스틱, 나노 플라스틱, 폴리스티렌, 내재화, 자궁 내막 기질 세포, 세포 독성, 세포 외 소포체, 전이